Electrodeposition of Ag/CNT Composite Films from Iodide Plating Baths

Journal of The Electrochemical Society, 2020 **167** 122515

Electrodeposition of Ag/CNT Composite Films from Iodide Plating Baths

Susumu Arai,[*,z] Taishi Kikuhara, Masahiro Shimizu,[*] and Masaomi Horita

Department of Materials Chemistry, Faculty of Engineering, Shinshu University, Wakasato, Nagano 380-8553, Japan

Ag/carbon nanotube (CNT) composite films were prepared by electrodeposition from non-cyanide baths. An iodide bath and multiwalled CNTs were used. The stability of the iodide bath under ambient conditions at various pH levels was examined, along with the changes in visual appearance, pH, and triiodide ion (I_3^-) concentration. The electrodeposition was conducted under galvanostatic conditions using iodide baths with and without CNTs. The microstructure of the Ag and Ag/CNT composite films was characterized, and the hardness, electrical conductivity, and coefficient of friction of the films were measured. The iodide bath was stable at higher pH levels under ambient conditions. The obtained Ag/CNT composite films exhibited a compact structure, and CNTs were homogeneously distributed in the interior of the deposited Ag matrix. The CNT content in the deposits increased with increasing CNT concentration in the plating bath. The hardness of the Ag/1.2 mass%-CNT composite film was 63.2 HV, which was slightly greater than that of the Ag film (60.4 HV). The resistivity of the composite film was 1.9 $\mu\Omega$ cm, which was slightly higher than that of the pure Ag film (1.8 $\mu\Omega$ cm). The coefficient of friction of the composite film was lower than that of the Ag film.
 [DOI: 10.1149/1945-7111/abb4ac]

Manuscript submitted July 13, 2020; revised manuscript received August 27, 2020. Published September 9, 2020.

Ag exhibits the highest electrical and thermal conductivities among all metals; consequently, Ag plating has been widely used for electrical contact parts as well as for the decoration of tableware. Recently, Ag-plated parts have been used for quick chargers for electric vehicles and in-vehicle battery peripherals. In general, the Ag plating process is carried out using a plating bath containing toxic cyanide compounds. The development of non-cyanide Ag plating baths is desirable and is an active research area. Ammonia,[1,2] thiosulfate,[3–5] succinimide,[6,7] uracil,[8] (*N*-(2-hydroxyethylene)ethylenediaminetriacetic acid,[9] 2-hydroxypyridine,[10] and 5,5-dimethylhydantoin[11] have been examined as alternative ligands for silver ions (Ag^+) to replace cyanide ions (CN^-). Iodide ions (I^-) also form stable complex ions with Ag^+, and studies on the electrodeposition of Ag using iodide baths have also been reported.[12–15]

In the recent literature, research on the Ag composite plating of electronic connectors using non-cyanide baths, such as Ag/carbon black composite plating using a 5,5-dimethylhydantoin bath[16] and Ag–W alloy/cobalt oxide composite plating using a hydantoin derivative bath,[17] has been reported. In these reports, the carbon black or cobalt oxide was used as a solid lubricant to reduce the coefficient of friction and the amount of wear. Carbon nanotubes (CNTs) also function as a solid lubricant,[18] and the lubricities of Ni–P alloy/CNT,[19–23] Cu/CNT,[24] Ni/CNT,[25,26] Co/CNT,[27] and Co–W alloy/CNT[28] composite films prepared by electroplating or electroless plating have been investigated. In the case of Ag/CNT composite plating, excellent electrical contact characteristics of the Ag/CNT composite film prepared using a cyanide bath have been reported.[29] The establishment of an eco-friendly Ag/CNT composite plating technology necessitates the development of Ag/CNT composite film fabrication methods that use non-cyanide baths.

In the present study, a stable iodide bath for the electrodeposition of Ag/CNT composite films was prepared and the microstructure of the electrodeposited Ag/CNT composite films was characterized. In addition, the electrical conductivity, hardness, and coefficient of friction of the composite films were evaluated.

Experimental

A Ag plating bath comprising 0.2 M AgI and 2.5 M KI was prepared. Immediately after preparation, the plating bath was colorless and transparent. However, the bath became yellow under ambient conditions because of the generation of I_2, which was formed by the oxidation of I^-.[30] To examine the stability of the bath under ambient conditions, three types of baths with different pH values (i.e., 1, unadjusted (9), and 12) were prepared. The bath pH was adjusted by dropping H_2SO_4 or KOH solutions into the baths. The unadjusted bath pH was ~9, represented as pH = 9 hereafter. Because I_2 readily reacts with I^- to form triiodide ions (I_3^-) (see Eq. 2), the I_3^- concentration was determined instead of the I_2 concentration. The changes in the appearance, pH, and I_3^- concentration of the plating baths were evaluated for 30 d under ambient conditions. The I_3^- concentration was measured using an iodide–-starch reaction.[31]

The CNTs used in the present study were commercially available vapor-grown multiwalled CNTs (Showa Denko Co. Ltd., VGCF-H). The CNTs were typically 100–150 nm in diameter and 10 μm in length. The Ag/CNT composite plating bath was prepared by adding CNTs to the Ag plating bath in the absence of a dispersant. A commercially available electrolytic cell (Microcell Model I, Yamamoto-Ms Co., Ltd.) with internal dimensions of 65 × 65 × 95 mm^3 was used for the electrodeposition. The volume of the plating bath was 300 cm^3. A pure Cu substrate (C1020) with an exposed surface area of 10 cm^2 (3 × 3.33 cm^2) was used as the substrate. Before the electrodeposition of Ag/CNT composite films as well as Ag films onto the Cu substrate, a Ag strike layer was applied to the Cu substrate to form a high-adhesion Ag layer. The Ag strike layer was deposited at a current density of 30 mA cm^{-2} using the aforementioned iodide bath at room temperature and without agitation. The electrical charge was 9 C cm^{-2}. The Ag/CNT composite film as well as the Ag film were then electrodeposited onto the Ag strike layer on the Cu substrate at a current density of 10 mA cm^{-2} at room temperature and with aeration. The aeration was carried out using an air pump (S101, Yamamoto-Ms Co. Ltd.). Cathode polarization measurements were conducted using an electrochemical measurement system (HZ-7000, Hokuto Denko) to clarify the electrodeposition behaviors of Ag from the iodide bath. A pure Ag plate was used as the working and counter electrodes. A Ag/AgCl electrode in saturated KCl (+0.199 V vs SHE) was used as the reference electrode. The measurements were performed at room temperature with and without aeration.

Microstructures of the deposited films were examined by field-emission scanning electron microscopy (FE-SEM; JEOL JSM-7000F). Exclusive sample preparation equipment (ion milling: Hitachi Hightech IM4000) was used to prepare cross-sectional

*Electrochemical Society Member.
[z]E-mail: araisun@shinshu-u.ac.jp

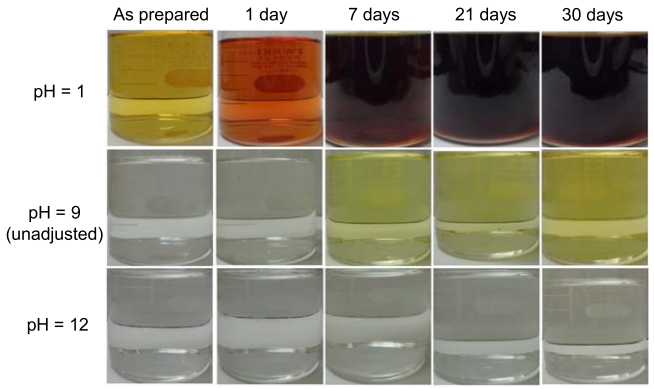

Figure 1. Change in appearance of Ag plating baths with different pH levels (1, unadjusted (9), 12) for 30 d.

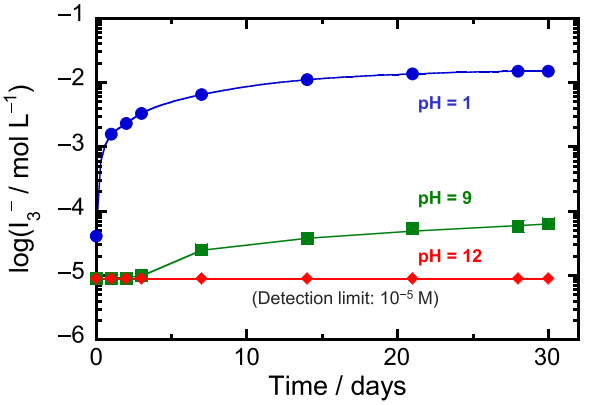

Figure 2. Time dependence of the triiodide-ion (I_3^-) concentration in pH-adjusted Ag plating baths.

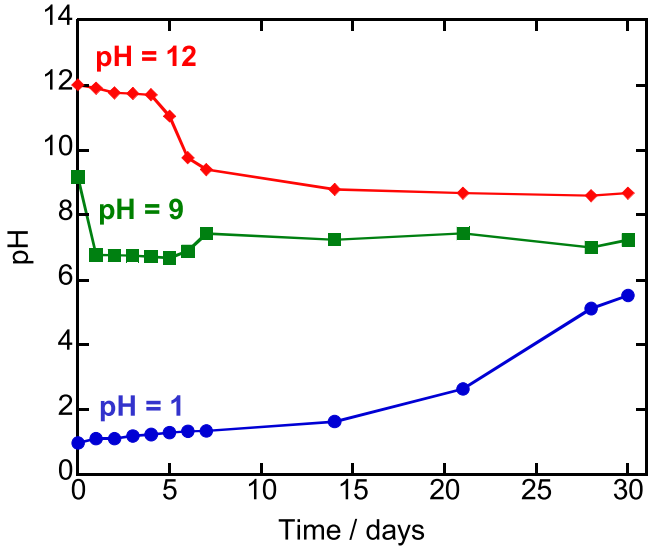

Figure 3. Time dependence of bath pH in pH-adjusted Ag plating baths.

samples for FE-SEM observation. The CNT content in the composite films was determined by direct weighing. For the weight measurement, thick Ag/CNT composite films (greater than 1.2 g) were electrodeposited onto a pure Cu (C1020) substrate without the Ag strike layer to form Ag/CNT composite films with low adhesion. After the composite film was exfoliated from the substrate, the Ag matrix of the composite film was dissolved in nitric acid (HNO_3). The CNTs in the HNO_3 solution were then filtered, dried, and weighed. The CNT content in mass% was calculated by dividing the mass of CNTs by that of the Ag/CNT composites. The CNT content in mass% was converted to that in volume% using Ag and CNT densities of 10.49 and 2.1 g cm^{-3}, respectively.

The phase structures of the films were examined by X-ray diffraction (XRD, Shimadzu Co. Ltd., XRD-6100). The crystallite size of the films was directly evaluated from the cross-sectional direction by electron backscatter diffraction (EBSD) using an apparatus (EDAX Co. Ltd., DigiView) attached to the FE-SEM. The hardness and the electrical resistivity of the films were measured using a micro-Vickers hardness tester (Shimadzu Co. Ltd., DUH-201) and a resistivity meter (Nitto Seiko Co. Ltd., Loresta-GP MCP-T610), respectively. The coefficient of friction of the films was measured using a ball-on-disk-type friction test machine (tribometer, Anton Paar, THT). An alumina ball (6 mm diameter, HV = 1500) was used as the counter-surface. Tests were conducted under a normal load of 1 N. All measurements were performed without using lubricants and under ambient conditions.

Results and Discussion

Figure 1 displays the transients of the appearance of the pH-adjusted iodide baths. The pH = 1 bath was yellow immediately after preparation, became orange after 1 d, then became reddish-brown after 7 d. The pH = 9 (unadjusted) bath was colorless immediately after preparation and gradually became yellow after 1 d. The pH = 12 bath was colorless for several days after preparation and became light-yellow after 7 d. Thus, the stability of iodide baths was strongly affected by their pH.

Figure 2 shows the time dependence of the I_3^- concentration in the pH-adjusted Ag plating baths. The lower detection limit of the I_3^- concentration by the iodine–starch method is 1×10^{-5} M. In the case of pH = 1, the I_3^- concentration increased drastically at the beginning and reached 1.5×10^{-2} M after 30 d. In the case of pH = 9, the I_3^- concentration increased gradually and reached 6×10^{-5} M after 30 d. By contrast, in the case of pH = 12, the I_3^- concentration was under the detection limit (1×10^{-5} M) even after 30 d. Thus, the changes in the appearances of the Ag plating baths in Fig. 1 are attributable to the formation of I_3^-.

Figure 3 shows the time dependence of pH in the pH-adjusted Ag plating baths. In the case of pH = 1, the pH increased with increasing exposure time and reached 5.2 after 30 d. In the case of pH = 9, the pH did not substantially change, remaining in the range 7–9. In the case of pH = 12, the pH changed to 9 after several days and remained constant thereafter.

In acidic aqueous solution, I^- ions are oxidized to I_2 by dissolved O_2[30]:

$$4I^- + O_2 + 4H^+ \rightleftharpoons 2I_2 + 2H_2O \quad [1]$$

The resultant I_2 easily reacts with I^- in the KI solution (i.e., the plating bath) to form I_3^-[30]:

$$I_2 + I^- \rightleftharpoons I_3^- \quad [2]$$

In the case of pH = 1, the increase of the pH must be due to the formation of I_2 and/or I_3^- according to Eqs. 1 and 2. The decrease in pH in the case of pH = 12 is likely due to the dissolution of atmospheric CO_2 into the Ag plating bath:

$$CO_2 + H_2O \rightleftharpoons H_2CO_3 \quad [3]$$

$$H_2CO_3 \rightleftharpoons H^+ + HCO_3^- \quad [4]$$

$$HCO_3^- \rightleftharpoons H^+ + CO_3^{2-} \quad [5]$$

This decrease in pH is likely related to the slight change in appearance of the bath in Fig. 1.

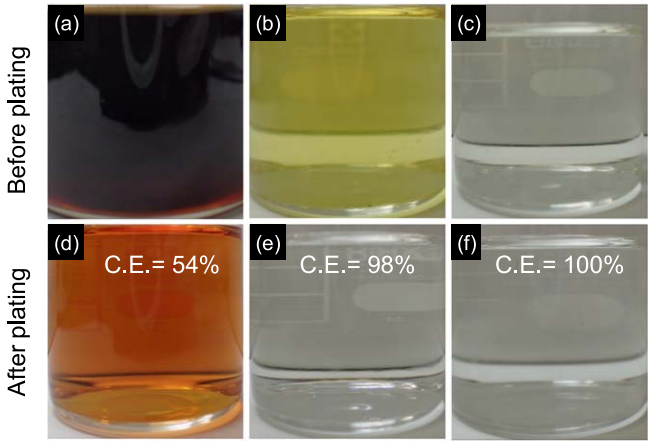

Figure 4. Appearance of Ag plating baths with different pH before and after electrodeposition of Ag. Baths left for 30 d under ambient conditions were used. (a)–(c) Appearances of the pH = 1, pH = 9 (unadjusted), and pH = 12 baths before electrodeposition, respectively. (d)–(f) Appearances of the pH = 1, pH = 9 (unadjusted), and pH = 12 baths after electrodeposition, respectively. The current efficiency (C.E.) for each bath is also shown in (d)–(f).

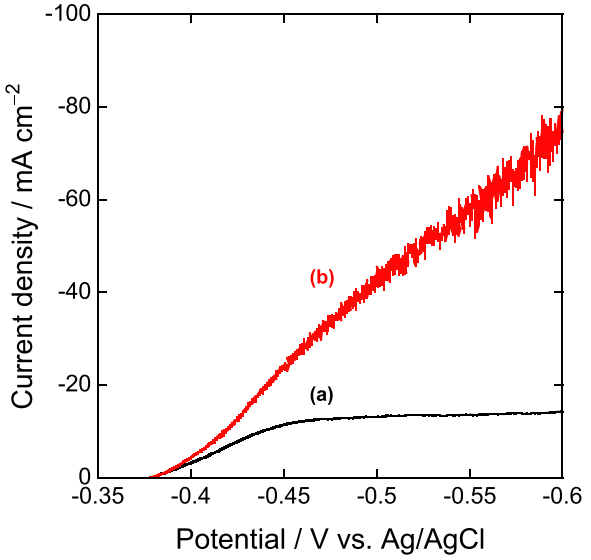

Figure 5. Current–potential curves for the electrodeposition of Ag from the pH = 12 baths (a) without and (b) with aeration.

In the case of pH = 9, the bath pH is presumably affected by the reactions represented in Eqs. 1–5, resulting in a pH in the range from 7 to 9.

The half-reaction and standard electrode potential of the I_2/I^- system are expressed as

$$I_2 + 2e^- \rightleftharpoons 2I^- \quad E^\circ = 0.53 \text{ V vs SHE} \qquad [6]$$

The half-reaction and standard electrode potential of the O_2/H_2O system in an acidic aqueous solution are

$$O_2 + 4H^+ + 4e^- \rightleftharpoons 2H_2O \quad E^\circ = 1.23 \text{ V vs SHE} \qquad [7]$$

The half-reaction and standard electrode potential of the O_2/OH^- system in a basic aqueous solution are

$$O_2 + 2H_2O + 4e^- \rightleftharpoons 4OH^- \quad E^\circ = 0.40 \text{ V vs SHE} \qquad [8]$$

From Eqs. 6 and 7, the spontaneous reaction and the standard cell potential in an acidic aqueous solution under standard conditions are

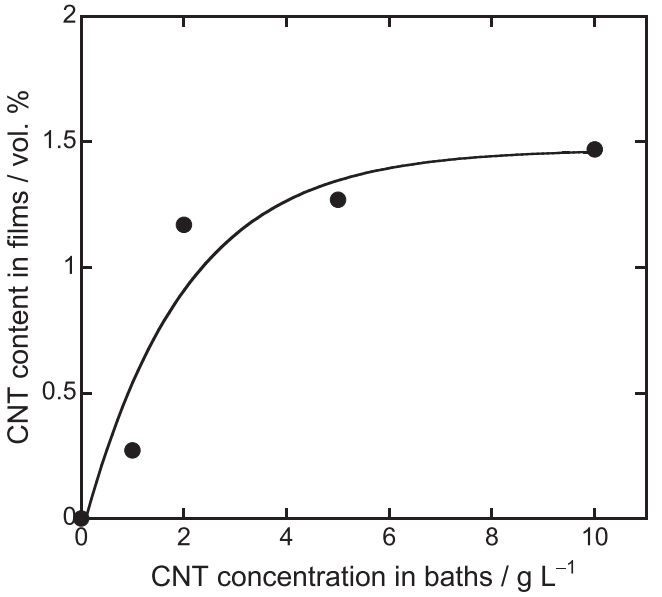

Figure 6. Relationship between the CNT concentration in the plating bath and the CNT content in the deposited film.

$$4I^- + O_2 + 4H^+ \rightarrow 2I_2 + 2H_2O \quad E^\circ_{cell} = 0.70 \text{ V} \qquad [9]$$

In contrast, from Eqs. 6 and 8, the spontaneous reaction and the standard cell potential in a basic aqueous solution under standard conditions are

$$2I_2 + 4OH^- \rightarrow 4I^- + O_2 + 2H_2O \quad E^\circ_{cell} = 0.13 \text{ V} \qquad [10]$$

Therefore, when the bath pH is adjusted to a high value such as 12, I^- is expected to not undergo spontaneous oxidation under the actual conditions, resulting in a stable plating bath.

The appearances of the pH-adjusted plating baths before and after the electrodeposition of Ag are shown in Fig. 4. Plating baths left for 30 d were used. In the case of pH = 1, the appearance changed from reddish-brown to orange. In the cases of pH = 9 and 12, the appearances changed from yellow to colorless and from light-yellow to colorless, respectively. The current efficiencies of the plating processes in the pH = 1, 9, and 12 baths were 54%, 98%, and 100%, respectively. During the electrodeposition of Ag from the Ag plating bath containing I_3^-, the reduction of I_3^- occurred in addition to the Ag electrodeposition, [30] resulting in the observed color changes of the plating baths. This reduction reaction of I_3^- also affected the current efficiency (C.E.). The C.E. of the Ag plating bath adjusted to pH = 12 was 100%; accordingly, the optimum pH of the Ag plating baths was determined to be 12 in the present study.

The electrodeposition behavior of Ag from the plating bath (pH = 12) is shown in Fig. 5. Figure 5a shows the current–potential curve without agitation. The increase of the current density due to the electrodeposition of Ag occurred at approximately −0.38 V vs Ag/AgCl, and the current density rapidly reached a limiting current density of −14 mA cm^{-2} at approximately −0.5 V. The limiting current density was maintained to −0.6 V vs Ag/AgCl. Figure 5b shows the current–potential curve recorded in the experiment with aeration. As in the experiment without agitation, the electrodeposition of Ag occurred at −0.38 V (Fig. 5a). However, compared with current-density curve (a) in Fig. 5, the curve corresponding to aeration (Fig. 5b) shows that the current density increased with increasing cathode overpotential to −0.6 V vs Ag/AgCl, reaching −75 mA cm^{-2} without a clear current plateau. The fluctuation of the current density is caused by the aeration. In the present study, because the same aeration was conducted and the applied current

density was 10 mA cm^{-2}, the electrodeposition of Ag most likely occurred under charge-transfer rate control.

The Ag/CNT composite plating bath was prepared by simply adding CNTs to the Ag plating bath at pH = 12. The aggregation of the CNTs was observed while the composite plating bath was standing. However, during the aeration, the CNTs were visually observed to homogeneously disperse.

Figure 6 shows the relationship between the CNT concentration in the plating bath and the CNT content in the deposited films. The CNT content in the films increased with increasing CNT concentration in the bath, approaching a plateau value at a CNT concentration of ~2 g l^{-1} in the bath. The maximum CNT content was 1.5 vol% when the CNT concentration was 10 g l^{-1}. The shape of the curve appeared to obey the well-known Langmuir adsorption isotherm.[32,33]

Surface and cross-sectional SEM images of the Ag/CNT composite film electrodeposited from the composite plating bath containing 2 g dm^{-3} CNTs are displayed in Fig. 7. Because this composite film contains 1.2 vol% CNTs (Fig. 6), it is referred as the Ag/1.2%-CNT film hereafter. For comparison, the surface and cross-sectional SEM images of the Ag film electrodeposited from the Ag plating bath (pH = 12) are shown in Figs. 7a and 7c, respectively. Numerous CNTs in non-aggregated form are observed on the surface of the electrodeposited Ag/1.2%-CNT film (Fig. 7b). Black regions in Fig. 7d are cross-sections of the CNTs. Thus, the CNTs are also distributed homogeneously across the interior of the deposited Ag matrix. Figures 7b and 7d also show that the CNTs exist in the composite film with random orientation.

Figure 8 shows XRD patterns of the Ag and Ag/1.2%-CNT films. Sharp diffraction peaks assigned to face-centered cubic Ag are observed in the patterns of both films (Fig. 8a). Figure 8b shows an enlargement of the XRD patterns in Fig. 8a in the 2θ range from 25 to 28°. An evident diffraction peak assigned to the graphite 002 plane is observed in the pattern of the Ag/1.2%-CNT film. This peak is due to the CNTs incorporated into the film.

Figure 9 displays the inverse pole figure (IPF) maps of the cross-sections of the Ag and the Ag/1.2%-CNT films. Figure 9a is the IPF map of the Ag film. Fine crystallites of deposited Ag smaller than 1 μm in diameter are observed on the Cu substrate. The diameter of the Ag crystallites increases with increasing film thickness and becomes greater than 10 μm at the film surface. The same texture is observed in the case of the Ag/1.2%-CNT film (Fig. 9b). Thus, even if the CNTs are incorporated into the film, the texture of the Ag matrix does not significantly change.

Table I shows the measurement results for the hardness and electrical resistivity of the Ag film and Ag/1.2%-CNT film. The hardness of the Ag/1.2%-CNT film is 63.2 HV, which is slightly higher than that of the Ag film (60.4 HV). Because the crystallite sizes of both the Ag film and Ag/1.2%-CNT film are approximately the same (Fig. 8), the increase of the hardness is likely due to a dispersion effect of the CNTs. The electrical resistivity of the Ag/1.2%-CNT film (1.8 $\mu\Omega$ cm) is slightly higher than that of the Ag film (1.9 $\mu\Omega$ cm). Because the electrical conductivity of CNTs is highly anisotropic as a consequence of their unique structure[34] and because the CNTs exist in the Ag/CNT film with random orientation (Figs. 7b and 7d), the CNTs in the composite film likely do not contribute to the improvement of the electrical conductivity of the composite film. Therefore, in the case of the Ag/1.2%-CNT film, most of the electricity should flow through the Ag matrix. Because the content of the CNTs is only 1.2 vol%, the Ag/1.2%-CNT film likely shows a slightly higher electrical resistivity than the Ag film. That is, the Ag/1.2%-CNT film has a slightly lower electrical conductivity than the Ag film.

Figure 10 shows the frictional behavior of the Ag/1.2%-CNT film; the frictional behavior of the Ag film is also displayed for comparison. The Ag film exhibited a coefficient of friction of ~0.65 from the beginning to the end of the wear test. By contrast, the coefficient of friction of the Ag/1.2%-CNT film at the beginning was ~0.25 and gradually increased to the final value of ~0.52. Thus, the Ag/1.2%-CNT film shows a lower coefficient of friction than the Ag film. The SEM images of the wear scars on the films after the wear test are shown in Fig. 11. A continuous scar is evident on the surface of the Ag film (Fig. 11a). By contrast, the wear scar of the Ag/1.2%-CNT film is discontinuous (Fig. 11b). Figures 11c and 11d show enlarged views of the scars of the Ag film and the Ag/1.2%-CNT film, respectively. Compared with the scar of the Ag film, numerous

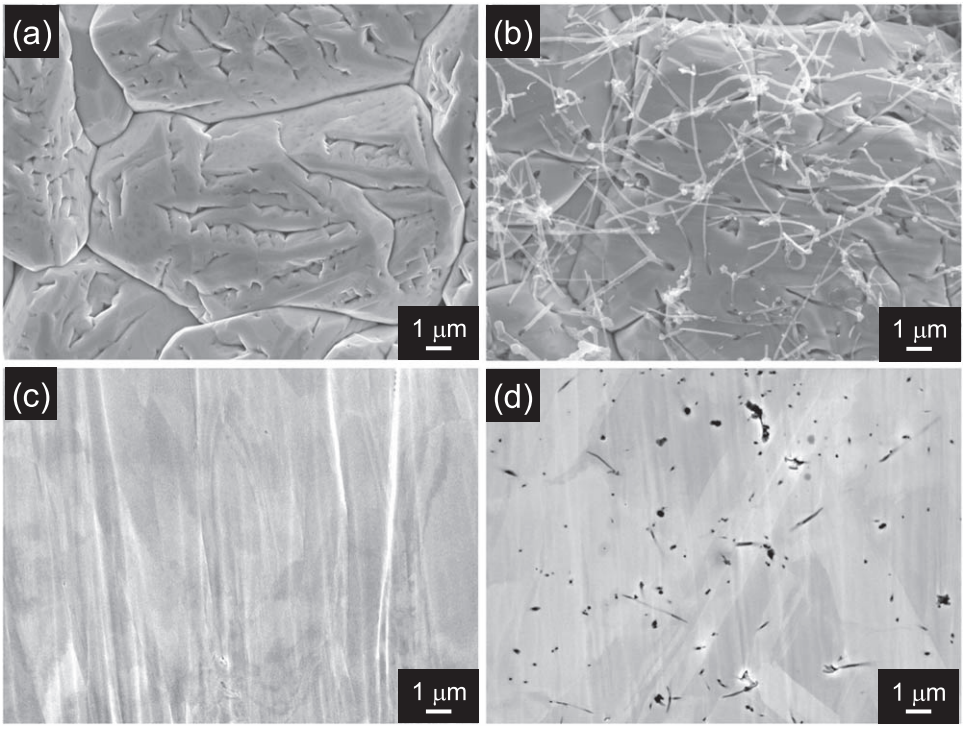

Figure 7. Surface and cross-sectional SEM images of the Ag film and Ag/CNT film: (a), (b) Surface SEM images of Ag and Ag/1.2%-CNT films, respectively; (c), (d) cross-sectional SEM images of Ag and Ag/1.2%-CNT films, respectively.

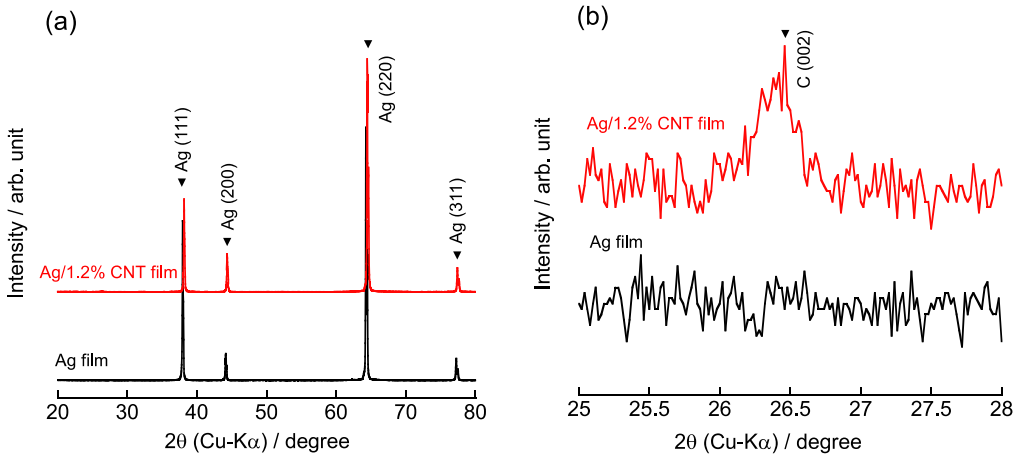

Figure 8. XRD patterns of Ag and Ag/1.2%-CNT films: (a) XRD patterns over a wide 2θ range (20°–80°); (b) enlarged XRD patterns showing the 2θ range from 25° to 28° in figure (a).

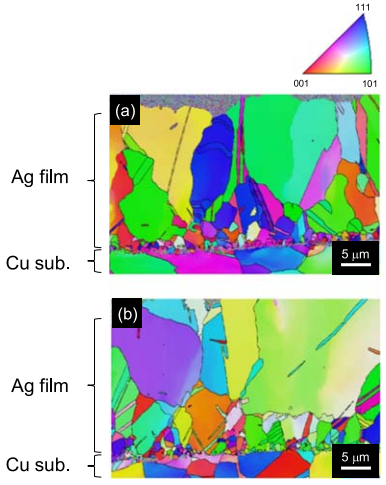

Figure 9. IPS mapping images of cross-sections of (a) a Ag film and (b) a Ag/1.2%-CNT film.

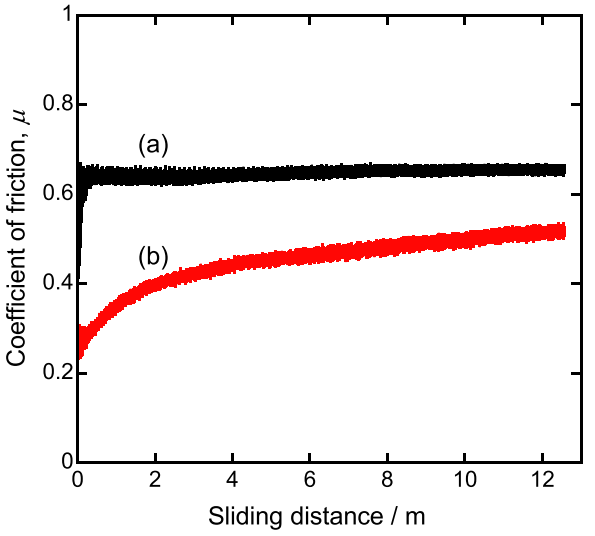

Figure 10. Transition of the coefficient of friction: (a) Ag film and (b) Ag/1.2%-CNT film.

Table I. Hardness and electrical resistivity of Ag and Ag/CNT films.

Sample	Hardness (HV)	Electrical resistivity ($\mu\Omega$ cmZ)
Ag film	60.4	1.8
Ag/1.2%-CNT film	63.2	1.9

CNTs are evident on the scar of the Ag/1.2%-CNT film. These CNTs most likely act as a solid lubricant, resulting in a lower coefficient of friction.

Conclusions

The stability of a Ag plating bath containing I^- as the ligand for Ag^+ was examined using pH as a parameter. The oxidation of I^- was suppressed with increasing pH; accordingly, the bath was stable at higher pH (pH = 12). A Ag/CNT composite plating bath was prepared by simply adding CNTs to the iodide bath (pH = 12), without the addition of surfactants. Ag/CNT composite films in which CNTs are distributed homogeneously were formed by electrodeposition. The hardness of the Ag/1.2%-CNT composite film was slightly higher than that of the Ag film, and the electrical conductivity of the composite film was slightly lower than that of the Ag film. The coefficient of friction of the Ag/1.2%-CNT composite film was evidently lower than that of the Ag/1.2%-CNT film because

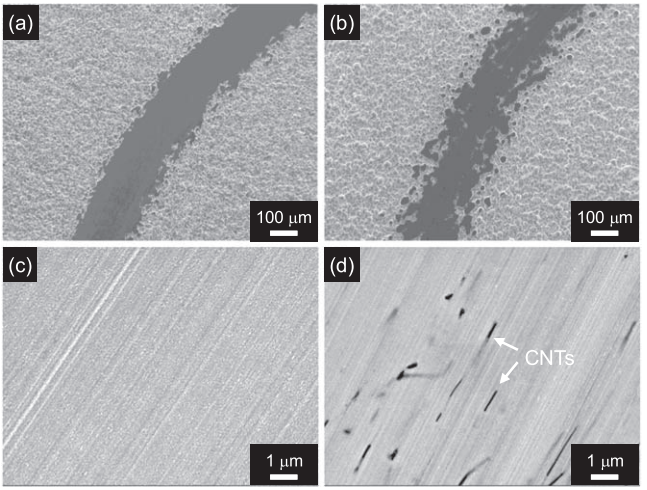

Figure 11. Surface SEM images of wear scars on the films after the wear test: (a) Ag film and (b) Ag/1.2%-CNT film; (c) enlarged picture of the scar area in figure (a); (d) enlarged image of the scar area in figure (b).

of the solid lubricity of the CNTs. We expect this Ag/CNT composite plating process using a non-cyanide bath to be used in the electric and electronics industries for the production of, for example, connector parts.

ORCID

Susumu Arai https://orcid.org/0000-0002-4915-0398
Masahiro Shimizu https://orcid.org/0000-0003-1084-7486

References

1. B. J. Polk, M. Bernard, J. J. Kasianowicz, M. Misakian, and M. Gaitan, *J. Electrochem. Soc.*, **151**, C559 (2004).
2. M. M. Hernandez and I. Gonzalez, *J. Electrochem. Soc.*, **151**, C220 (2004).
3. S. Sriveeraraghavan, R. M. Krishnan, and S. R. Natarajan, *Met. Finish.*, **87**, 115 (1989).
4. W. Simons, D. Gonnissen, and A. Hubin, *J. Electroanal. Chem.*, **433**, 141 (1997).
5. D. G. Foster, Y. Shapir, and J. Jorne, *J. Electrochem. Soc.*, **150**, C375 (2003).
6. S. Jayakrishman, S. R. Natarajan, and K. I. Vasu, *Met. Finish.*, **94**, 12 (1996).
7. S. Masaki, H. Inoue, and H. Honma, *Met. Finish.*, **96**, 16 (1998).
8. B. G. Xie, J. J. Sun, Z. B. Lin, and G. N. Chen, *J. Electrochem. Soc.*, **156**, D79 (2009).
9. G. M. de Oliveira, M. R. Silva, and I. A. Carlos, *J. Mater. Sci.*, **42**, 10164 (2007).
10. Z. B. Lin, B. G. Xie, J. S. Chen, J. J. Sun, and G. N. Chen, *J. Electroanal. Chem.*, **633**, 207 (2009).
11. A. Liu, X. Ren, B. Wang, J. Zhang, P. Yang, J. Zhang, and M. An, *RSC Adv.*, **4**, 40930 (2014).
12. K. P. Batashev and B. G. Kitaichik, *Tsvethykh Metal*, **188**, 239 (1957).
13. H. Inoue, K. Yamakawa, and S. Masaki, *J. Surf. Finish. Soc. Jpn.*, **41**, 1178 (1990).
14. H. Inoue, K. Yamakawa, and S. Masaki, *J. Surf. Finish. Soc. Jpn.*, **44**, 55 (1993).
15. O. A. Ashiru, *Plat. Surf. Finish.*, **82**, 76 (1995).
16. L. Stappers, C. N. Ngoy, W. Zhang, M. Toben, and J. Fransaer, *J. Electrochem. Soc.*, **160**, D137 (2013).
17. N. Dadvand and M. Dadvand, *J. Electrochem. Soc.*, **161**, D730 (2014).
18. P. L. Dickrell, S. K. Pal, G. R. Baurne, C. Muratore, A. A. Voevodin, P. M. Ajayan, L. S. Schadler, and W. G. Sauyer, *Tribol. Lett.*, **24**, 85 (2006).
19. W. X. Chen, J. P. Tu, L. Y. Wang, H. Y. Gan, Z. D. Xu, and X. B. Zhang, *Carbon*, **41**, 215 (2003).
20. X. H. Chen, C. S. Chen, H. N. Xiao, H. B. Liu, L. P. Zhou, S. L. Li, and G. Zhang, *Tribol. Int.*, **39**, 22 (2006).
21. Z. H. Li, X. Q. Wang, M. Wang, F. F. Wang, and H. L. Ge, *Tribol. Int.*, **39**, 953 (2006).
22. S. Arai, T. Sato, and M. Endo, *Surf. Coat. Technol.*, **205**, 3175 (2011).
23. Y. Suzuki, S. Arai, and M. Endo, *J. Electrochem. Soc.*, **157**, D50 (2010).
24. S. Arai and T. Kanazawa, *Surf. Coat. Technol.*, **254**, 224 (2014).
25. J. Tan, T. Yu, B. Xu, and Q. Yao, *Tribol. Lett.*, **21**, 107 (2006).
26. S. Arai, A. Fujimori, M. Murai, and M. Endo, *Mater. Lett.*, **62**, 3545 (2008).
27. S. Arai and K. Miyagawa, *Surf. Coat. Technol.*, **235**, 204 (2013).
28. S. Arai and K. Miyagawa, *ECS J. Solid-State Sci. Technol.*, **2**, M39 (2013).
29. M. Fujishige, M. Sekino, K. Fujisawa, S. Morimoto, K. Takeuchi, S. Arai, and A. Kawai, *Appl. Phys. Express*, **3**, 065801 (2010).
30. S. Masaki, M. Yoshimoto, H. Inoue, and H. Honma, *J. Surf. Finish. Soc. Jpn.*, **49**, 84 (1998).
31. R. E. Rundle and D. French, *J. Am. Chem. Soc.*, **65**, 1707 (1943).
32. N. Guglielmi, *J. Electrochem. Soc.*, **119**, 1009 (1972).
33. H. Hayashi, S. Izumi, and I. Tari, *J. Electrochem. Soc.*, **140**, 362 (1993).
34. A. M. Abyzov, S. V. Kindalov, and F. M. Shakhov,, *J. Mater. Sci.*, **46**, 1424 (2011).